Enhancing SNR by Anisotropic Diffusion for Brillouin Distributed Optical Fiber Sensors

Kuo Luo, Biwei Wang, Nan Guo, Kuanglu Yu, *Member, IEEE, Member, OSA,*

Changyuan Yu, *Senior Member, IEEE, Senior Member, OSA, and Chao Lu, Fellow, OSA*

***Abstract*—Anisotropic diffusion (AD) is employed to enhance the signal-to-noise ratio (SNR) of Brillouin distributed optical fiber sensor. A Brillouin optical time-domain analyzer (BOTDA) with 99-km-long fiber under test is set up, where a section of 2.3 m and another 182 m section at the end of the fiber are heated for experimental verification. The SNR of experimental data sets with different sampling point numbers are enhanced to several improvement levels by AD and three other methods for comparison. Results show that the 2.3 m section and the temperature transition region of the 182 m section are better preserved by AD than other methods for the same SNR improvement. Objective criteria analysis shows that AD achieves the best measured spatial resolution and temperature accuracy among the four methods, the location of temperature transition can be detected more accurately for data with low SPNs after AD denoising. In addition, the processing time of AD is 1/3 that of non-local means (NLM) and 6‰ that of block-matching and 3D filtering (BM3D). The edge-preserving quality and fast processing speed allow the proposed algorithm to be a competitive denoising alternative for sensors based on Brillouin scattering.**

***Index Terms*—Brillouin distributed optical fiber sensor, spatial resolution, noise reduction, anisotropic diffusion.**

I. Introduction

In recent years, technology of Brillouin distributed optical fiber sensing has attracted a lot of attention [1]-[3] and has been applied in various fields [4]-[7]. This technology realizes long-distance and high-accuracy measurements detection of the strain and temperature based on the principle that Brillouin frequency shift (BFS) is linearly related to the change of strain and temperature [8].

Signal-to-noise ratio (SNR) of the sensing signal limits the performance of Brillouin distributed optical fiber sensor, including spatial resolution, sensing accuracy and sensing distance, *etc* [9], [10]. Many techniques have been used to enhance SNR, including distributed Raman amplification [11], optical pulse coding (OPC) [12], image processing [13]-[18], *etc*., in which image processing can filter out the noise without extra configuration of equipment. In Ref. [13], wavelet shrinkage based one-dimensional (1D) wavelet denoising (WD) decreased measurement time meanwhile reducing the noise in Brillouin gain spectrum (BGS) compared with the normal averaging technique. Two dimensional (2D) image restoration algorithms including 2D WD and non-local means (NLM) were used by Soto [14] to intensify the response of distributed optical fiber sensors and improved the performance by 100 times in shorter time for additive white Gaussian noise (AWGN) filtering. A repeater-less Brillouin optical time-domain analyzer (BOTDA) system with a sensing range of 157.8 km was set up by Lewis [15]. Then, NLM was used and compared with OPC technique and the result showed the better performance of using NLM. It was proved by Qian [16] that NLM based on noise level estimation algorithm can remove the noise of the sensing system without signal distortion. In Ref. [17], SNR was improved using NLM for a coherent BOTDA system without trace averaging. Block-matching and 3D filtering (BM3D) algorithm was proposed by Wu [18] and proved to maintain the best measurement accuracy and experimental spatial resolution compared with NLM and WD but with much higher computation complexity.

In this manuscript, we propose to use anisotropic diffusion (AD) to enhance the SNR of the Brillouin distributed optical fiber sensor. The most striking feature of AD is that it can retain and even enhance the edge of image while reducing the noise. Since 1990 when it was proposed by Perona and Malik [19], AD has been widely used in many areas, such as denoising of magnetic resonance image (MRI) [20] and synthetic aperture radar image [21]. The transition region of BGS caused by variation of temperature or strain can be regarded as an edge of the 2D spectrum image. AD can maintain the information of the region while removing the noise, which gives rise to less distortion on measured spatial resolution and frequency accuracy. In the experiments, Lorentzian curve fitting (LCF) is

This work was supported in part by the National Natural Science Foundation of China (NSFC) under Grant 61805008, in part by the Fundamental Research Funds for the Central Universities under Grant 2020YJS043, in part by the GRF 15200718 from UGC of Hong Kong and in part by Outstanding Chinese and Foreign Youth Exchange Program of China Association of Science and Technology. *(Corresponding author: Kuanglu Yu.)*

K. Luo and K. Yu are with Institute of Information Science, Beijing Key Laboratory of Advanced Information Science and Network Technology, Beijing 100044, China (e-mail: 14281013@bjtu.edu.cn; klyu@bjtu.edu.cn).

B. Wang, C. Yu and C. Lu are with the Department of Electronic and Information Engineering, The Hong Kong Polytechnic University, Kowloon, Hong Kong (e-mail: biwei.wang@connect.polyu.hk; changyuan.yu@polyu.edu.hk; chao.lu@polyu.edu.hk).

N. Guo is with the College of Optoelectronic Engineering, Chongqing University, Chongqing, China (e-mail: guonan@cqu.edu.cn).

K. Luo and B. Wang contributed equally to this work.

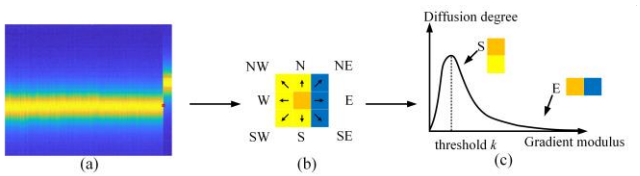

Fig. 1. (a) BGS data with the tail section heated; (b) Diffusing towards 8 adjacent points; (c) Relationship between gradient modulus and diffusion degree.

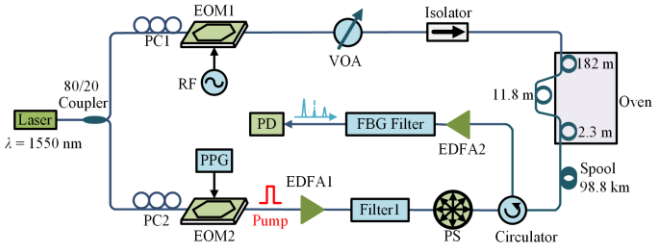

Fig. 2. BOTDA experiment setup, PC: Polarization Controller, EOM: Electro-Optic Modulator, PPG: Pulse Pattern Generator, RF: Radio Frequency, PS: Polarization Scrambler, VOA: Variable Optical Attenuator, EDFA: Erbium-doped Fiber Amplifier, PD: Photodetector, FBG: Fiber Bragg Grating.

used to acquire temperature. Sampling point number (SPN) and SNR are two variables for the experimental processing and several performance parameters related to Brillouin distributed sensor are discussed. Three most advanced algorithms are used as comparison for experiments. And the results of experiments show that AD has a competitive performance on the measured criteria. We believe that the algorithm is helpful for theoretical research and practical applications in Brillouin and other distributed fiber sensor systems for SNR enhancing.

II. Theory

In image processing, the idea of diffusion comes from the multi-scale description of images which can be theoretically regarded as isotropic heat diffusion equation [22], but isotropic diffusion can blur image edges while filtering out noise. To address this issue, the anisotropic diffusion was proposed by Perona and Malik [19]:

$$\begin{cases} \dfrac{\partial I}{\partial t} = div(g(\|\nabla I\|)\cdot\nabla I) \\ I(t=0)=I_0 \end{cases} \tag{1}$$

where ∇ is the gradient operator; $\|\nabla I\|$ is the modulus of the gradient; *div* is the divergence operator; I_0 is the raw image which represents the raw data in this manuscript; $g(\|\nabla I\|)$ is the diffusion coefficient and otherwise known as the edge-stopping function. The diffusion coefficient has two forms [19]:

$$g(\|\nabla I\|) = \frac{1}{1+(\|\nabla I\|/k)^2} \tag{2}$$

$$g(\|\nabla I\|) = \exp[-(\|\nabla I\|/k)^2] \tag{3}$$

where k is the gradient threshold. The difference between the two equations is that the first privileges wide regions over smaller ones, the second prefers high-contrast edges over low-contrast ones.

Equation (1) needs to be discretized, with brightness values associated to the Brillouin gain spectrum. 8-nearest-neighbors discretization of (1) is used in our case and can be expressed as:

$$\begin{aligned} I^{t+1} = I^t + \lambda[&g_N\cdot\nabla_N I + g_S\cdot\nabla_S I + g_E\cdot\nabla_E I \\ &+ g_W\cdot\nabla_W I + g_{NW}\cdot\nabla_{NW} I + g_{NE}\cdot\nabla_{NE} I \\ &+ g_{SE}\cdot\nabla_{SE} I + g_{SW}\cdot\nabla_{SW} I]^t \end{aligned} \tag{4}$$

where $0 \le \lambda \le 1/8$; *N*, *S*, *E*, *W*, *NW*, *NE*, *SE*, *SW* are subscripts for North, South, East, West, Northeast, Northwest, Southeast, Southwest, respectively; t represents the preset iterative numbers. The symbol $\bigtriangledown$ (different with the symbol ∇, which is the gradient operator) indicates the nearest-neighbor differences:

$$\bigtriangledown I_{p,q} \equiv I_p - I_q, \forall q \in \eta_p \tag{5}$$

where p represents the coordinate for the point in the data matrix; η_p means the neighbors of point p. For each point in the 2D data set, the diffusion result was influenced by the neighboring 8 points in our experiments, and Perona and Malik used 4-nearest-neighbors discretization as an example to show the properties of anisotropic diffusion in Ref. [19] while we find out 8 neighbors discretization is better in our experiment after multiple attempts. More neighbors may also could be used at the increase of the computational complexity.

In our case, the BGS data is treated as a 2D matrix as shown in Fig. 1(a). The tail section of the fiber is put into the oven to generate a temperature transition. For any point in the matrix, its adjacent points have effects on it. The degree of the effects is related to the magnitude of the gradient modulus value $\|\nabla I\|$ between the point and its adjacent points. Here, the border part in the transition region of the BGS is shown in Fig. 1(b). The energy of orange and yellow points is much higher than that of the blue ones. The gradient modulus value of the orange point along a specific direction is approximately represented by the energy difference between the point and its adjacent point in this direction. Then, the non-negative monotonically decreasing diffusion coefficient $g(\|\nabla I\|)$ is then used. Normally, the gradient modulus value of an edge is much larger than the gradient threshold k, so the result of the diffusion equation is approximately equal to zero, which means that the diffusion is inhibited just like diffusing towards E direction shown in Fig. 1(c). In contrast, for a flat region, when the noise level approaches the threshold k, the diffusion is enhanced, shown as the S direction in Fig. 1(c). The basic principle of AD is to use gradient threshold k to distinguish the image gradient change caused by noise and by edge, and neighborhood weighted averaging is then utilized to remove the small gradient change caused by noise and retain the large gradient change caused by edge. This process is iterative to the preset number t [23].

III. Experiments

A. Experimental setup

The proposed algorithm is applicable to all sensors based on Brillouin scattering and even those based on other scatterings with a waterfall map. BOTDA is taken as an example in this manuscript.

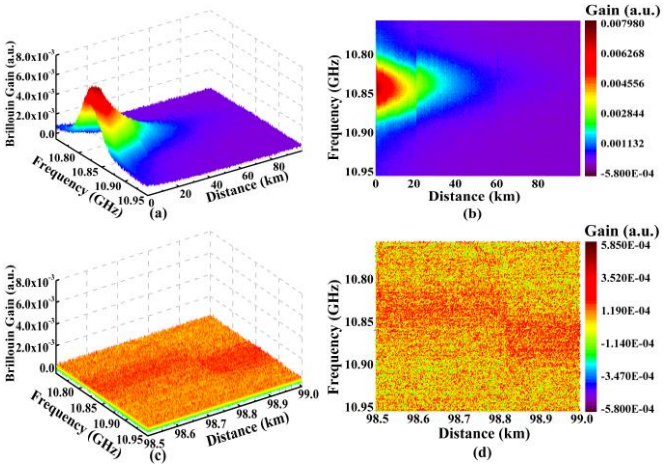

Fig. 3. (a) and (b) Measured BGS distribution along FUT without denoising; (c) and (d) last 500 m of the FUT without denoising; Both the 2.3 m section at 98.803 km and the 182 m section are heated to 60.3 ℃.

TABLE I
OPTIMAL PARAMETERS FOR DENOISING ALGORITHMS

Algorithms	Parameters	Settings
WD	Wavelet	Sym5
	Decomposition level	5
	Threshold strategy	Hard
NLM	Similarity window size	3 * 3
	Search window size	13 * 13
BM3D	Sliding step	2
	Block size	12 * 12
	Search window size	13 * 13
	Max matched blocks	16
	Threshold strategy	Hard&Wiener
AD	Diffusion equation	(2)
	Diffusion constant	1/8
	Diffusion times	10

The experimental setup of the BOTDA system is shown in Fig. 2 [24], [25]. Light from a continuous wave (CW) laser operating at 1550 nm is split by an 80/20 coupler into two branches to generate the pump and probe signals. The CW light at the upper branch with the radio frequency (RF) signal applied to the electro-optic modulator (EOM1) provides the dual sideband probe signal with the original carrier suppressed over 30 dB. A variable optical attenuator (VOA) is used to control the probe light power before the probe enters the fiber under test (FUT) and the isolator followed blocks the signal from the reverse direction. The signal at the lower branch is modulated by the EOM2 driven by a pulse pattern generator (PPG) to generate pump pulse with extinction ratio over 40 dB. The Erbium-doped fiber amplifier (EDFA1) is used to increase the peak pump power and the filter1 is used to remove the amplified spontaneous emission (ASE) noise. A polarization scrambler (PS) is used before the pulse entering the FUT to suppress the polarization dependent noise. The probe signal experienced the stimulated Brillouin scattering (SBS) is then amplified by EDFA2 and detected by a photo detector (PD) after the unwanted higher frequency sideband is filtered out by a fiber Bragg grating (FBG) filter.

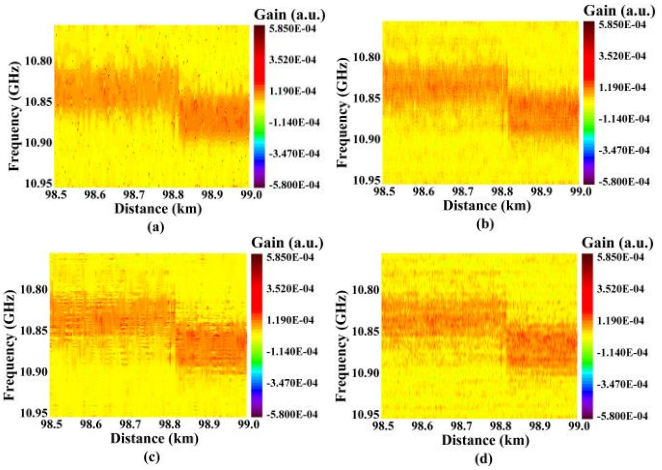

Fig. 4. Measured BGS of the last 500 m section along FUT with SNR improvement of 16 dB by (a) WD, (b) NLM, (c) BM3D and (d) AD.

In the experiments, the collection of data is carried out in two stages. At first stage, the data along the 99 km fiber with 20 ns pump pulse was collected with 2000 averaging. Then, the low SNR data along the last 500 m section under the pump pulse of 2 ns which means a 0.2 m spatial resolution with only 200 averaging was recorded, so that we can store and process only the noisy data at the tail part to save time. The bandwidth of the PD is 125 MHz and the frequency scanning range is from 10.751 to 10.950 GHz with a step of 1 MHz. A 99-km-long single mode fiber without strain is used as the FUT and the raw data acquired from the BOTDA is shown in Figs. 3(a) and 3(b). The FUT is spliced by three sections, which can be seen clearly in Fig. 3(b). The last 500 m spool of the FUT is shown in Figs. 3(c) and 3(d), in which a 2.3 m section at the location of 98.803 km and a 182 m section at the end of the FUT heated to 60.3 ℃ are depicted. Because of low SNR at the end of the FUT, the range of the color bar in Figs. 3(c) and 3(d) is set differently from that in Figs. 3(a) and 3(b) to show the heated section obviously.

B. Data processing and algorithm parameters

As two important parameters, SNR and SPN affect the performance of noise reduction algorithms [18]. In order to study the performance of the proposed method under low SPN, the raw data of the last 500 m section is dropped at equal intervals along the optical fiber direction and five data sets with SPNs of 10, 8, 6, 4 and 2 within 2 m section are thus obtained. Then 2D WD, NLM, BM3D and AD are applied to denoise those data respectively. Here we use 2D WD instead of the 1D WD, as the former is more efficient in dealing with the data replicated in different dimensions [14]. The performance of four algorithms can be evaluated by objective criteria, including root-mean-square error (RMSE), error of temperature transition location, measured spatial resolution, measured temperature accuracy and processing speed. The denoising performance of different algorithms are analyzed with the same SNR improvement for fairness. For each data set, the average SNR of the set is calculated and then increased to different improvements. In our experiments, four SNR improvements are adopted, *i.e.*, 4, 8, 12 and 16 dB, achieved by setting the level

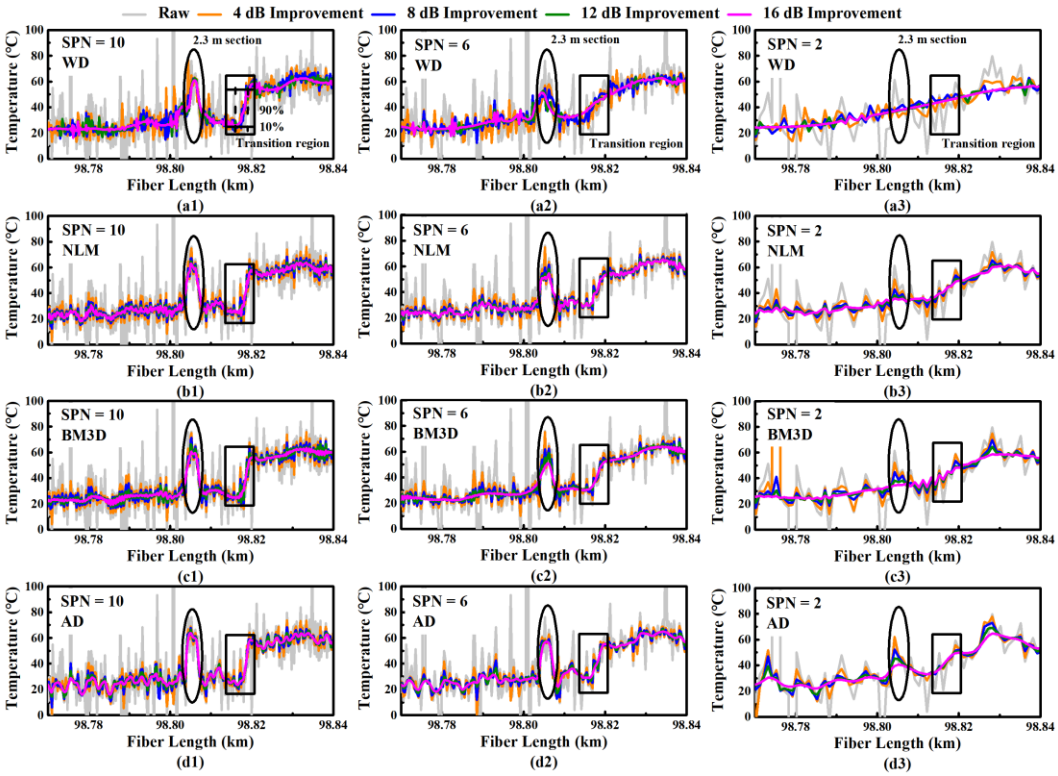

Fig. 5. Temperature distribution around the 2.3 m section at the location of 98.803 km and the last 182 m temperature transition region by using (a) WD, (b) NLM, (c) BM3D and (d) AD for denoising with different SPNs, respectively.

of threshold in the denoising algorithms. Here, the SNR is calculated using the method in Ref. [26].

The thresholds of denoising algorithms are adjusted for different SPN data sets to reach good performance. In 2D WD, the wavelet threshold varies from 1.935σ to 3.285σ where σ is the estimated standard deviation (SD) of the noise in the obtained data with different SPNs. In this manuscript, a patch-based estimation algorithm proposed in Ref. [16] is used to acquire the noise level of the BGS. In NLM, the smoothing control parameter is set between 0.73σ and 2.36σ, while in BM3D the threshold is adjusted from 0.6σ to 1.14σ, and in AD, the gradient threshold is from 0.37σ to 1.8σ. According to the optimization procedures reported in Ref. [14], [16], [18], the optimal parameters in Table I are adopted. In this manuscript, parameters of BM3D are further optimized to have faster processing speed and better performance.

IV. Results

In Figs. 4(a)-4(d), BGS distributions along the last 500 m FUT with SNR improved by 16 dB using 2D WD, NLM, BM3D and AD are demonstrated, respectively, where the SPN of the plotted data is 10. Compared with the raw data in Figs. 3(c) and 3(d), both the 2.3 m section and the last 182 m heated section can now be clearly recognized.

After denoising, LCF is employed and the corresponding temperature distribution is calculated according to the BFS-temperature coefficient of the FUT. Fig. 5 shows the temperature distribution around the 2.3 m section at the location of 98.803 km circled by black ellipse and temperature transition region of the last 182 m section of the FUT marked by black square area. All four denoising algorithms are used to enhance the SNR for BGS of different SPNs, respectively. SPNs of 10, 6 and 2 are shown for better illustration in Fig. 5, while we have tested five data sets with SPN decreasing from 10 to 2 in a step of 2. The gray lines depict the results without denoising which serve as a reference. The orange, blue, green and pink lines depict the results after denoising when the SNR is improved by 4, 8, 12 and 16 dB, respectively. Each row in Fig. 5 shows that the measured temperature of the 2.3 m section is getting lower and lower with the rise in SNR. From Figs. 5(a1)-5(a3), we can see that with the SPN decreasing from 10 to 2, the measured temperature of the 2.3 m section is gradually decreasing, and the peaks in the 2.3 m section region almost disappear after denoising by 2D WD when SPN decreases to 2 as shown in Fig. 5(a3). The same thing occurs in Figs. 5(b3) and Figs. 5(c3), which are denoised by NLM and BM3D, respectively. As for AD, we can still see the peaks in the 2.3 m section in Fig. 5(d3) which means AD can effectively retain 2.3 m section heated region even with SNR improvement of 16 dB and SPN of 2.

It is easy to find out that the lines in the temperature transition region are smoothed with the increasing of SNR. From each row of Fig. 5, the smoothness is becoming more and more obvious with the decreasing of SPN for all the four algorithms. In Figs. 5(a2), 5(b2), 5(c2) and 5(d2), 2D WD has an obvious smoothness compared with other three algorithms at the same SNR improvement when SNP decreases to 6. In addition, the lines in temperature transition region have been completely smoothed by 2D WD denoising in Fig. 5(a3) when only 4 dB SNR is improved, which means big degradation of the

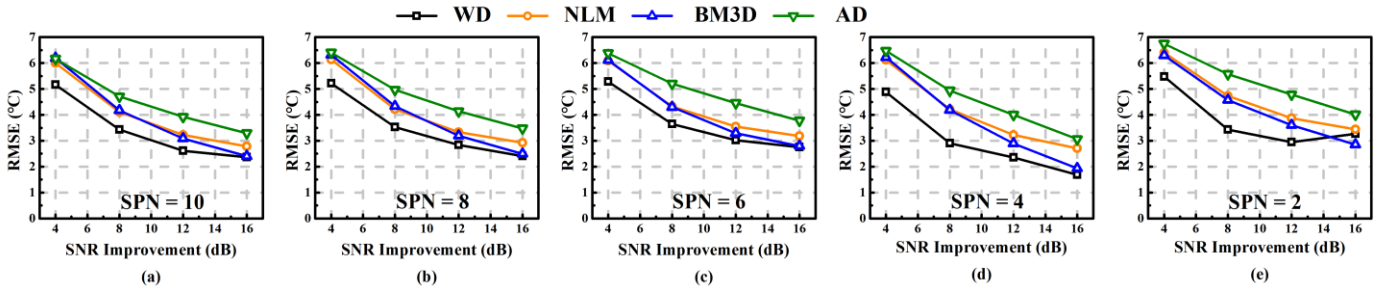

Fig. 6. RMSE for the last 182 m fiber heated to 60.3 ℃ with SNR improved by 2D WD, NLM, BM3D and AD when SPNs are (a) 10, (b) 8, (c) 6, (d) 4 and (e) 2 within 2 m section, respectively.

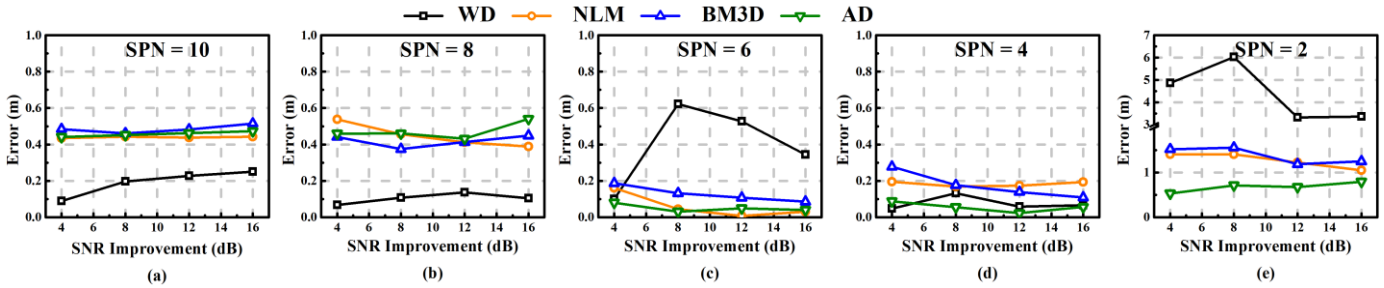

Fig. 7. Error of the location of temperature transition with SNR improved by 2D WD, NLM, BM3D and AD when SPNs are (a) 10, (b) 8, (c) 6, (d) 4 and (e) 2 within 2 m section, respectively.. Note that the range of the Y-axis of (e) is different from those in (a)-(d).

measured spatial resolution and much error of the measured temperature transition location. The same thing happens in Figs. 5(b3) and 5(c3) when NLM and BM3D are used for denoising. As for AD, it effectively protects the edges in Fig. 5(d3), which represents the temperature transition region in our case, even under SPN of 2.

After the acquisition of the temperature data, denoising performance can be analyzed by objective criteria mentioned above. Firstly, RMSE is calculated by comparing the actual temperature with the measured temperature along the last 182 m heated section of the FUT extracted by LCF [27]. The RMSE of all cases of five different SPNs are computed and the results are shown in Fig. 6. The black squares, orange dots, blue triangles and green triangles depict the RMSE of the data after denoising by 2D WD, NLM, BM3D and AD, respectively. Because the noise level of the raw data is high, the RMSE of the results after LCF is large at first, as the SNR improving, the RMSE is getting smaller. And 2D WD provides the smallest RMSE compared with the other three methods for each SPN while AD unfortunately achieves the largest RMSE in contrast. This can be explained as peaks in BGS caused by high level noise sometimes are retained by AD, which leads to the increase in RMSE, whilst the same peaks will be smoothed by the other three methods. Luckily, various AD based advanced algorithms can be used to further improve the performance in RMSE for our proposed algorithm which will be discussed later.

Then, measured location of the temperature transition is calculated. The fiber under room temperature and the spool heated in oven along the last 182 m section are selected separately to calculate averages respectively. Then, points along the rising edge, of which the number equals SPN, are selected to fit into a linear line. Then the start and end location of the temperature transition region can be determined on the rising edge with the averages calculated before, and the middle of the start and end location is then calculated which represents our measured transition location. The absolute value of the difference between the measured transition location and its actual location which related to the middle point of the transient is calculated as the error of the measured location. The error of the location of temperature transition for all cases of SPNs are shown in Fig. 7. It should be noted that the range of the Y-axis in Fig. 7(e) is different from those in Figs. 7(a)-7(d) because the error increases rapidly when SPN decreases to 2. From Figs. 7(a) and 7(b), 2D WD has the smallest error, and NLM, BM3D and AD almost have the same degree of error when SPN decreases from 10 to 8. When SPN continues to decrease from 6 to 2, AD always has the minimal error of the measured temperature transition location, it can detect the transition location more accurately than the other three algorithms at low SPNs.

For measured spatial resolution, the fitting process for the rising edge is the same as the calculation of the location of the temperature transition location, and the distance from 10% to 90% of the rising edge is selected as the measured spatial resolution [18] which is shown in Fig. 5(a1). The result is affected by various factors, including noise level of the raw data, noise reduction effect, fitting points selection, *etc*., thus it changes dramatically in some cases. Fig. 8 depicts the comparison of measured spatial resolution among the four algorithms for all 5 cases of SPNs. The insets in Figs. 8(a) and 8(b) show details about the results. It should be again noted that the range of the Y-axis of Fig. 8(e) is different from the others as the measured spatial resolution increases rapidly with the decreasing of SPN. It is easy to know from Fig. 8 that with the improvement of SNR, the measured spatial resolution shows an upward trend for most cases. Although irregular trends exist in several cases, *i.e*., all the line segments in Fig. 8(b) and black

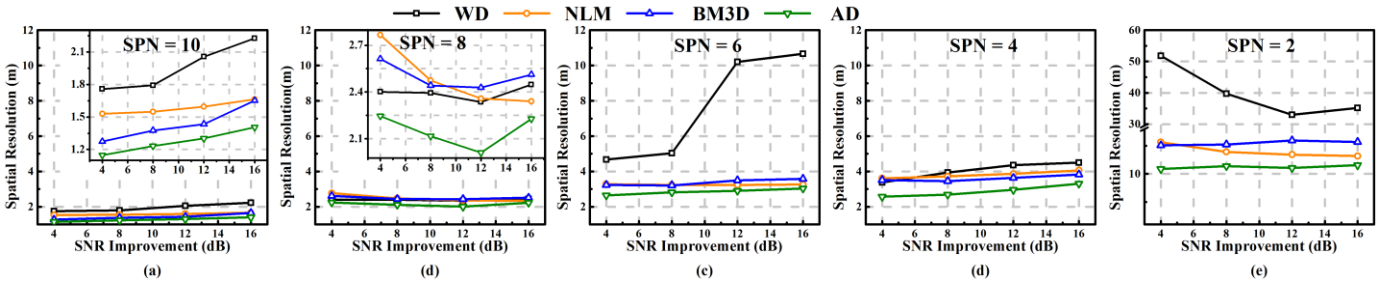

Fig. 8. Measured spatial resolution with SNR improved by 2D WD, NLM, BM3D and AD when SPNs are (a) 10, (b) 8, (c) 6, (d) 4 and (e) 2 within 2 m section, respectively. Insets in (a) and (b) show more details. Note that the range of the Y-axis of (e) is different from those of (a)-(d).

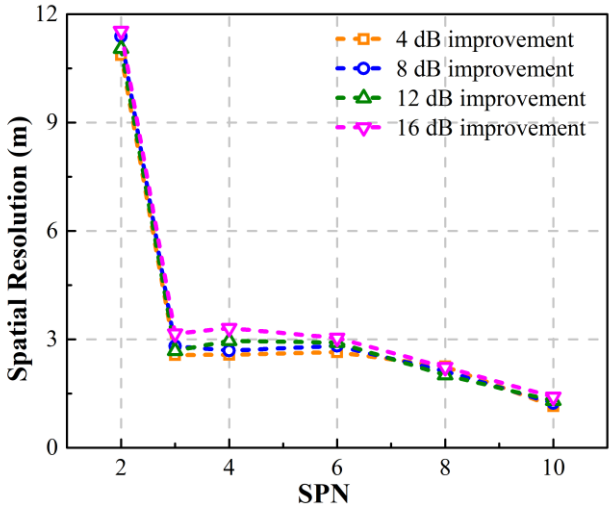

Fig. 9. Measured spatial resolution degradation of data with different SPNs (2, 3, 4, 6, 8, 10) denoised by AD algorithm with different SNR improvements.

line segment in Fig. 8(e), we can still draw a conclusion that data denoised by AD algorithm always has the minimum measured spatial resolution for each SPN.

Noting that the spatial resolution increases largely when the SPN goes below 4, we want to further study the performance of the noise reduction algorithms under low SPN to avoid the performance loss. As previous experimental results have shown that all the experimental noise reduction algorithms perform poorly in terms of measured spatial resolution at low SPN (especially SPN equals to 2), we take AD which performs the best among the four methods as an example here. As illustrated in Fig. 9, when SPN decreases from 10 to 3, the measured spatial resolution increases gradually and slightly when SNR improvements ranging from 4 to 16 dB. When SPN equals to 2, spatial resolution experienced a dramatic degradation which may partially be resulted from the limitation of the number of points used for the fitting of the rising edge (transition area). Besides, it's also important to note that the error of the transition location and the measured temperature of the 2.3 m section also have a large loss in accuracy when the SPN equals to 2. While those criteria can be guaranteed when the SPN is 3, therefore, in order to avoid a large degradation of the performance for denoising methods, it's recommended to use the data of which the SPN is larger than 2.

TABLE II
PROCESSING TIME COMPARISON OF DIFFERENT DENOISING ALGORITHMS

	SPN				
	2	4	6	8	10
2D WD	0.01s	0.01s	0.02s	0.03s	0.03s
NLM	0.24s	1.12s	1.7s	2.23s	2.77s
BM3D	33.56s	48.89s	89.58s	98.91s	124.13s
AD	0.06s	0.41s	0.55s	0.72s	0.85s

Next, the average temperature along the 2.3 m heated section is calculated for measured temperature accuracy. And the results are shown in Fig. 10. The red dashed lines depict the actual temperature of the 2.3 m section. In Fig. 10, it is obvious to know that measured temperature gradually deviates from the oven temperature of 60.3 ℃ with the SNR improvement for all four methods for each SPN. As for data denoising by AD, shown as the green line segments in Fig. 10, have the least deviation with the same SNR improvement compared with the other three methods. It's necessary to mention that we used the average of the 2.3 m as the measured temperature, and with the SPN decreases, the actual point number for averaging in the 2.3 m heated section decreases from 10 to 2 in our experiments. There are also some other methods to measure the temperature accuracy, for instance, taking the maximum as the measured temperature or the average temperature of the same point under the same situation over several measurements, *etc*. After data processing, we find that those methods may be helpful to reduce the decline of the resulting peak hot-spot temperatures, but the trend in Fig. 10 for four mentioned methods will not change.

Finally, the computational speed of AD is analyzed and compared with the other three algorithms. Here, we use a computer with Intel ® Core i7-8700 CPU @ 3.20 GHz and RAM of 24 GB and implement the above algorithms in PyCharm 2019. For the data size of the last 500 m section is 2500 * 200, the processing time is recorded for all cases of SPNs. For each algorithm, average of processing time for four SNR improvements for each data set is calculated and shown in Table II. It's obvious that BM3D takes over two magnitudes higher processing time, while 2D WD has the least processing time for each SPN. And the processing time of AD is short as well, which is about 1/3 that of NLM and only 6‰ that of BM3D.

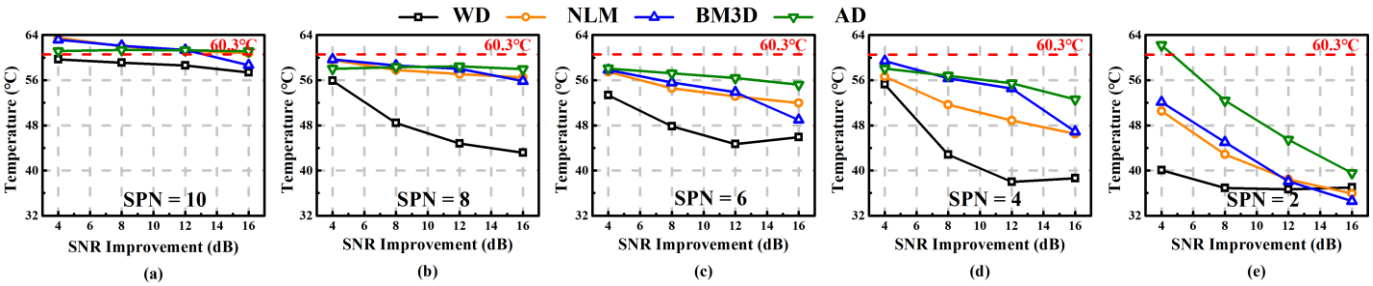

Fig. 10. Measured average temperature of the 2.3 m heated section with SNR improved by 2D WD, NLM, BM3D and AD, when SPNs are (a) 10, (b) 8, (c) 6, (d) 4 and (e) 2 within 2 m section, respectively.

V. Discussion

In this section, the characteristics of the denoising algorithms and especially AD related ones are further discussed.NLM is a spatial-domain filter which depends on the similarity of the multidimensional data. WD uses wavelet transform to filter out the noise in BOTDA. BM3D employs both the non-local redundancy and transform-domain filtering for denoising. Compared with those advanced filtering techniques, AD does not require complicated transform of images and can be regarded as the diffusion towards adjacent directions in a 2D matrix. Therefore, for the points in the matrix, the factors affecting their changes only come from its adjacent points, which is the opposite to the non-locality. This allows AD to preserve the edge by controlling the diffusion degree of a point along different directions just according to the energy difference between the point and its adjacent points. It also explains why AD has lower computation complexity than NLM and BM3D.

In this manuscript, four common criteria of the BOTDA was introduced to give the proposed method a fair comparison with another 3 advanced methods. Taking those criteria into consideration, it's hardly possible to find a denoising method that could always obtain the best performance for the four proposed criteria. What we focus on is to find out the right scenario for those methods to show their best performance. For instance, if the temperature or the frequency accuracy is required accurately, then WD will be the best solution as shown in Fig. 6, while if the edge information or the spatial resolution is precisely needed, then AD will be the choice. In our case, the transition area of the acquired data is sharp, as temperature transferred from 25 ℃ to 60.3 ℃. While when the longitudinal temperature transition is not as steep as in this manuscript, *i.e.* characterized by small gradients, and the proposed AD method could not distinguish noise from the edge and will introduce a heavy loss in performance. Since it is difficult to obtain the data of low temperature difference due to our oven could not work steadily at least 10 degrees higher than environmental temperature, we simulated the experiments. The results show that the minimum temperature difference to keep the proposed method's performance is found to be about 8.5 ℃, or around 8 MHz.

As a suggestion for future investigation, pointed out by the authors of Ref. [28], denoising process along the BGS (frequency) direction will bring no decisive improvement on the BFS estimation and the accuracy of the BFS can be improved by processing the data along the fiber direction. Parameters which control the diffusion direction along fiber direction should be chosen with more care for future improvement of our proposed method. And the classical AD algorithm mentioned above could be further improved with advanced AD algorithms as well. As mentioned in section III, the classical AD proposed by Perona and Malik is more suitable to deal with low level noise, while for high level noise, various advanced models, including Catté_PM [29], anisotropic median diffusion (AMD) [30], *etc*., may be exploited. In addition, the denoising performance is also influenced by the gradient threshold k of AD, which is acquired by a patch-based noise estimation algorithm in this manuscript. Then a robust anisotropic diffusion algorithm proposed in Ref. [31] which can estimate the threshold automatically using robust statistics [32] may be useful.

VI. Conclusion

In this manuscript, AD is introduced to enhance the SNR for Brillouin distributed optical fiber sensor. A BOTDA of 99 km FUT with a section of 2.3 m and another section of 182 m heated in oven is set up. The raw data acquired from the BOTDA system is dropped at equal intervals along the optical fiber direction to obtain data sets with different SPNs (10, 8, 6, 4 and 2) in order to analyze the effect of SPN on the proposed algorithm. AD and another three advanced methods, including 2D WD, NLM and BM3D, are employed to denoise for data sets with different SPNs. LCF is then used to acquire the temperature, four criteria are introduced to analyze the performance of the four methods.

Experimental results show that the proposed method can effectively decrease the noise for BGS. The temperature acquired by LCF after AD denoising provides better measured temperature accuracy and spatial resolution than the other three methods with the same SNR improvement for each data set. Unfortunately, AD achieves the largest RMSE in the experiment because its edge-preserving characteristic makes it retains both the edges caused by transition and by high level noise. Luckily, advanced AD models can be used to improve the performance in RMSE for the proposed method. The results also show that data sets after AD denoising can get the location of the temperature transition location more accurately than the other three methods at low SPNs. Finally, the processing speed of AD is compared with the other three algorithms and results

show that AD is much faster than NLM and BM3D. Therefore, the proposed anisotropic diffusion algorithm can be a competitive alternative for Brillouin distributed optical fiber sensor denoising.

ACKNOWLEDGMENT

The authors would like to thank Assoc. Prof. Yanyan Zhu of Beijing Jiaotong University for revising the language of this manuscript.

REFERENCES

[1] A. Motil, A. Bergman, and M. Tur, "State of the art of Brillouin fiber-optic distributed sensing," *Opt. Laser Technol*., vol. 78, pp. 81–103, 2010.

[2] X. Bao and L. Chen, "Recent progress in Brillouin scattering based fiber sensors," *Sensors*, vol. 11, no. 4, pp. 4152–4187, 2011.

[3] Z. Zhao, M. A. Soto, M. Tang, and L. Thévenaz, "Distributed shape sensing using Brillouin scattering in multicore fibers," *Opt. Express*, vol. 24, no. 22, pp. 25211–25223, 2016.

[4] J. M. Lopez-Higuera, L. Rodriguez Cobo, A. Quintela Incera, and A. Cobo, "Fiber Optic Sensors in Structural Health Monitoring," in *J. Lightwave Technol*., vol. 29, no. 4, pp. 587-608, Feb. 2011.

[5] M. Nikles, L. Thevenaz, and P. A. Robert, "Brillouin gain spectrum characterization in single-mode optical fibers," *J. Lightwave Technol*., vol. 15, pp. 1842-1851, 1997.

[6] H. Liang, X. Zhang, X. Li, and Y. Lu, "Design and implementation of data fitting algorithm for Brillouin back scattered-light spectrum data," *Acta Photonica Sinica*, vol. 38, no. 4, pp. 875-879, 2009.

[7] C. A. Galindez-Jamioy and J. M. Lopez-Higuera, "Brillouin distributed fiber sensors: An overview and applications," *J. Sens*., vol. 2012, pp. 1-17, 2012.

[8] T. Horiguchi, K. Shimizu, T. Kurashima, M. Tateda, and Y. Koyamada, "Development of a distributed sensing technique using Brillouin scattering," *J. Lightwave Technol*., vol. 13, no. 7, pp. 1296–1302, 1995.

[9] M. A. Soto and L. Thevenaz, "Modeling and evaluating the performance of Brillouin distributed optical fiber sensors," *Opt. Express*, vol. 21, no. 25, pp. 31347–31366, Dec. 2013.

[10] A. Denisov, M. A. Soto, and L. Thévenaz, "Going beyond 1000000 resolved points in a Brillouin distributed fiber sensor: theoretical analysis and experimental demonstration," *Light Sci*., vol. 5, no. 5, pp. 1–8, 2016.

[11] M. N. Alahbabi, Y. T. Cho, and T. P. Newson, "150-km-range distributed temperature sensor based on coherent detection of spontaneous Brillouin backscatter and in-line Raman amplification," *JOSA B*, vol. 22, no. 6, pp. 1321-1324, 2005.

[12] M.A. Soto *et al.*, "Simplex-coded BOTDA fiber sensor with 1 m spatial resolution over a 50 km range," *Opt. Lett*., vol. 35, no. 2, pp. 259–261, 2010.

[13] M. A. Farahani, M. T. V. Wylie, E. Castillo-Guerra, and B. G. Colpitts, "Reduction in the number of averages required in BOTDA sensors using wavelet denoising techniques," *J. Lightwave Technol*., vol. 30, no. 8, pp. 1134–1142, 2012.

[14] M. A. Soto, J. A. Ramirez, and L. Thévenaz, "Intensifying the response of distributed optical fibre sensors using 2D and 3D image restoration," *Nature Communications*, vol. 7, pp. 10870, Mar. 2016.

[15] X. Qian *et al.*, "157km BOTDA with pulse coding and image processing," in *Sixth European Workshop on Optical Fibre Sensors*, vol. 9916, pp. 99162S, May. 2016.

[16] X. Qian, Z. Wang, W. Sun, B. Zhang, Q. He, H. Wu, and Y. Rao, "Non-local means denoising based on noise level estimation for BOTDA," in *15th International Conference on Optical Communication and Networks*, 2016.

[17] N. Guo, L. Wang, H. Wu, C. Jin, H. Y. Tam, and C. Lu, "Enhanced Coherent BOTDA System without Trace Averaging," *J. Lightwave Technol*., pp. 99, 2017.

[18] H. Wu, L. Wang, Z. Zhao, N. Guo, C. Shu, and C. Lu, "Brillouin optical time domain analyzer sensors assisted by advanced image denoising techniques," *Opt. Express*, vol. 26, no. 5, pp. 5126-5139, 2018.

[19] P. Perona and J. Malik, "Scale-Space and Edge Detection Using Anisotropic Diffusion," *IEEE Transactions on Pattern Analysis and Machine Intelligence*, vol. 12, no. 7, pp. 629-639, Jul. 1990.

[20] G. Gerig *et al.*, "Nonlinear anisotropic filtering of MRI data," *IEEE Transactions on medical imaging*, vol. 11, no. 2, pp. 221-232, 1992.

[21] Q. Huang *et al.*, "A new anisotropic diffusion method for SAR speckle reduction," *Acta Electronica Sinica*, vol. 34, no. 9, pp. 1553-1557, 2006.

[22] J. Koenderink, "The structure of images," *Biological Cybernetics*, pp. 363-370,1984.

[23] J. H. Yu and Y. Y. Wang, "Image noise reduction based on anisotropic diffusion: A survey," *Journal of Electronic Measurement and Instrument*, vol. 25, no. 2, pp. 105-116, 2011.

[24] Z. Cao, N. Guo, M. Li, K. Yu, and K. Gao, "Back propagation neutral network based signal acquisition for Brillouin distributed optical fiber sensors," *Opt. Express*, vol. 27, no. 4, pp. 4549-4561, 2019.

[25] Y. Mao, N. Guo, K. Yu, H. Tam, and C. Lu, "1-cm-spatial-resolution Brillouin optical time-domain analysis based on bright pulse Brillouin gain and complementary code," *IEEE Photonics J*., vol. 4, no. 6, pp. 2243–2248, 2012.

[26] A. K. Azad, F. N. Khan, W. H. Alarashi, N. Guo, A. P. T. Lau, and C. Lu, "Temperature extraction in Brillouin optical time-domain analysis sensors using principal component analysis based pattern recognition," *Opt. Express*, vol. 25, no. 14, pp. 16534–16549, 2017.

[27] A. K. Azad *et al*., "Signal processing using artificial neural network for BOTDA sensor system," *Opt. Express* vol. 24, pp. 6769-6782, 2016.

[28] S. Zaslawski, Z. Yang, and L. Thévenaz, "On the 2D Post-Processing of Brillouin Optical Time-Domain Analysis," *J. Lightwave Technol*., to be published, 2020.

[29] F. Catté *et al*., "Image selective smoothing and edge detection by nonlinear diffusion," *SIAM Journal on Numerical Analysis*, vol. 29, no. 3, pp. 845-866, Jun. 1992.

[30] H. Ling and A. C. Bovik, "Smoothing low-SNR molecular images via anisotropic median-diffusion," *IEEE Transactions on Medical Imaging*, vol. 21, no. 4, pp. 377-384, 2002.

[31] M. J. Black *et al.*, "Robust anisotropic diffusion," *IEEE Transactions on Image Processing*, vol. 7, no. 3, pp. 412-432, 1998.

[32] P. J. Rousscuw and A. M. Leroy, "Robust regression and outlier detection," John Wiley & sons, vol. 589, 2005.